ELSEVIER

Comput. Methods Appl. Mech. Engrg. 167 (1998) 369–391

Computer methods in applied mechanics and engineering

A monolithical fluid–structure interaction algorithm applied to the piston problem

Frederic J. Blom

Institut de Machines Hydrauliques et Mécanique des Fluides, Ecole Polytechnique Fédérale de Lausanne, CH-1015 Lausanne, Switzerland

Received 3 February 1998; revised 22 April 1998

Abstract

An investigation of time marching computational fluid–structure interaction algorithms is presented. The analysis is applied to the piston problem. Attention is focussed on the time integration properties of the coupling algorithms. The staggered scheme is first investigated where fluid and structure are alternately integrated by separate solvers in a predictor–corrector fashion. This algorithm suffers from a time lag between the integration of the fluid and structure. The influence of the time lag is investigated by the comparison of different predictions for the structure. A novel monolithical algorithm is then introduced in order to annihilate the time lag. This algorithm integrates fluid, structure and interaction as a single system by an implicit algorithm. Linear acoustic as well as nonlinear Euler equations for gas dynamics are investigated. The numerical results of the staggered scheme reveal a non-physical deviation of the mean position of the piston at higher CFL numbers. The deviation of the mean position is not present in the calculation with the monolithical scheme. Stability analysis shows the unconditional stability of the monolithical scheme for the acoustic equations whereas the staggered scheme has a limited domain of stability. This domain can be enlarged by an improvement of the structural prediction. Analysis of the damping shows an energy production in the staggered scheme while the monolithical scheme has no energy production term. The analyses lead to the formulation of the Interaction Consistency Law which prescribes the relation for the time discretisation between fluid and structure solvers and their boundary conditions. © 1998 Elsevier Science S.A. All rights reserved.

1. Introduction

In order to calculate fluid–structure interaction in a time marching fashion both fluid and structure have to be integrated in time simultaneously. Often the problem is solved by means of a staggered algorithm. The fluid and structure are then alternatingly integrated in time by separate solvers. The interaction is taken into account by the boundary conditions. The drawback of this method is that there always exists a time lag between the integration of fluid and structure. Bendiksen [1] has shown that this can lead to a loss of dynamic equivalence between the aero-elastic model and the numerical algorithm.

The staggered method is introduced by Park et al. [2]. The method is used for transonic flutter calculations by Prananta et al. [3,4] and for incompressible fluid-structure interaction by Mouro [5]. Staggering of fluid and structure solvers is included in the algorithm by Piperno [6,7]. This algorithm makes use of the characteristic time scales in fluid and structure solvers by choosing different time steps for both solvers. This latter method is adopted by Blom and Leyland [8,9]. Piperno et al. [10] and Farhat et al. [11] have investigated different parallel versions of the staggered schemes. An analysis of predictor–corrector algorithms with structural as well as fluid predictions is presented by Prananta and Hounjet [12]. Staggered schemes are also investigated by Giles for aero-elastic problems [13] and thermo-elastic problems [14]. He addresses the accuracy and numerical stability of staggered schemes with several fluid and structure solvers.

Another interaction algorithm was proposed by Bendiksen [15] where the fluid and structure are integrated in time by an explicit fourth order Runge–Kutta scheme. There, the interaction between fluid and structure is also updated at every intermediate time level. This method was also applied by He [16] to a cascade flutter problem.

0045-7825/98/$19.00 © 1998 Elsevier Science S.A. All rights reserved.
PII: S0045-7825(98)00151-0

The accuracy of this algorithm is superior to the standard staggered algorithm since the interval between information exchange is decreased. However, the method remains staggered.

Recently, implicit fully coupled algorithms have gained more interest. This interest is driven by the need for larger time steps, hence a reduction of the computational time. Alonso and Jameson [17] and Melville et al. [18] used an implicit algorithm to integrate the fluid and structure in time. The nonlinear system of equations is solved by an iterative Newton solver. To obtain full coupling they updated the interaction after every subiteration. The influence of the number of subiterations in this algorithm is investigated by Morton et al. [19]. This algorithm also remains essentially staggered. It converges to a fully coupled scheme when the number of subiterations is increased.

In this paper a monolithical algorithm is proposed in order to avoid the time lag related to staggered schemes. One single operator is applied to the fluid, structure and mesh variables to integrate the complete system in time. This operator contains the integration of the fluid, mesh, structure and interaction. The algorithm is thoroughly investigated and compared to several staggered algorithms. In order to concentrate on the coupling algorithm, the relatively simple piston problem is studied. The piston problem is described by a one-dimensional equation for the fluid and a one degree of freedom system for the structure.

2. Piston problem

In this section the piston problem is investigated analytically. The results are used to validate the numerical algorithms. The piston problem consists of a tube filled with a compressible fluid. The left-hand side of the tube is closed and on the right-hand side the piston is placed. This piston has a mass m and is supported by a linear spring with stiffness k. The configuration is depicted in Fig. 1.

The fluid in the tube is considered to be inviscid and compressible. It is assumed to vary only in the x direction. Then the fluid is described by the one-dimensional Euler equations which read in conservative form

$$\frac{\partial}{\partial t}\begin{Bmatrix}\rho\\ \rho u\\ \rho E\end{Bmatrix}+\frac{\partial}{\partial x}\begin{Bmatrix}\rho u\\ \rho u^2+p\\ u(\rho E+p)\end{Bmatrix}=0 \tag{1}$$

where ρ, u, E and p denote the density, velocity, total energy and pressure, respectively. The equations are closed by the equation of state for a perfect gas

$$p=(\gamma-1)\rho\left[E-\frac{1}{2}(u^2)\right] \tag{2}$$

where γ is the ratio of the specific heats.

The boundary conditions for the fluid are given by

$$\begin{aligned}u(x=0)&=0\\ u(x=L)&=\dot{u}_s\end{aligned} \tag{3}$$

where $\dot{u}_s$ is the velocity of the piston.[1]

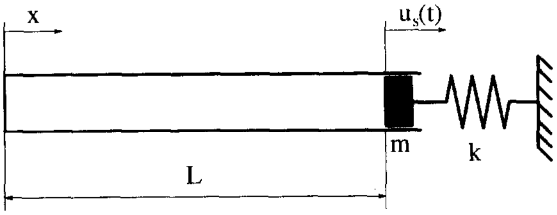

Fig. 1. Piston problem.

[1] The structure variables are denoted by the subscript s.

The movement of the piston is described by the undamped equation of motion for a one degree of freedom model,

$$m\ddot{u}_s(t) + ku_s(t) = f(t) \tag{4}$$

where $u_s(t)$, $\ddot{u}_s(t)$ are the displacement of the structure (piston) and its double time derivative, respectively. $f(t)$ is the external force. This external force is equal to the pressure difference between both sides of the piston multiplied by the piston surface,

$$f(t) = (p_L - p_a)\text{area} \tag{5}$$

where p_a is the ambient pressure and p_L is the pressure at $x = L$. Unit area is chosen for the piston.

In order to linearise the Euler equations (1), the variables are written as a mean value and an added perturbation. The following notations are introduced

$$\begin{aligned} \rho &= \bar{\rho} + \rho' \\ u &= \bar{u} + u' \\ p &= \bar{p} + p' \end{aligned} \tag{6}$$

where $\bar{\rho}$, $\bar{u}$ and $\bar{p}(= p_a)$ are the steady mean parts and ρ', u' and p' are the time dependent parts of the variables. To linearise the equations the following approximations are made

$$\begin{aligned} &\rho' \ll \bar{\rho} \\ &u' \ll c_s \\ &p' \ll \bar{p} \\ &\bar{u} = 0 \end{aligned} \tag{7}$$

where c_s is the isentropic speed of sound defined by

$$c_s^2 = \left.\frac{\partial p}{\partial \rho}\right|_s \tag{8}$$

Substituting (6), (7) and (8) in (1) and neglecting higher-order terms gives

$$\begin{aligned} &\frac{\partial p'}{\partial t} + \bar{\rho}c_s^2 \frac{\partial u'}{\partial x} = 0 \\ &\bar{\rho}\frac{\partial u'}{\partial t} + \frac{\partial p'}{\partial x} = 0 \end{aligned} \tag{9}$$

The linearised energy equation at isentropic conditions is always satisfied and is therefore omitted. Then, the first equation of (9) is differentiated with respect to time and the second with respect to space. This gives after subtraction a Helmholtz equation for the pressure,

$$\frac{\partial^2 p'}{\partial x^2} - \frac{1}{c_s^2}\frac{\partial^2 p'}{\partial t^2} = 0 \tag{10}$$

Now, Eqs. (4) and (10) with their boundary conditions have to be solved. First, a harmonic time dependence ($p' = \mathrm{p}\,e^{i\omega t}$ and $u_s = \mathrm{u}\,e^{i\omega t}$) is introduced. Then, the two equations read,

$$\begin{aligned} &\frac{\partial^2 \mathrm{p}}{\partial x^2} + \kappa^2 \mathrm{p} = 0 \\ &-\omega^2 m\mathrm{u} + k\mathrm{u} = \mathrm{p} \end{aligned} \tag{11}$$

where $\kappa(= \omega/c_s)$ is the wave number. The solution for the pressure equation is given by

$$\mathrm{p} = C_1\, e^{i\kappa}x + C_2\, e^{-ik}x \tag{12}$$

The integration constants have to be determined by the boundary conditions at both sides of the tube. These boundary conditions read

$$\left.\frac{\partial \mathrm{p}}{\partial x}\right|_{x=0} = 0$$
$$\left.\frac{\partial \mathrm{p}}{\partial x}\right|_{x=L} = -\rho\omega^2 \mathrm{u} \tag{13}$$

The coupled eigenfrequencies of the piston problem are found by solving Eqs. (11), (12) and (13). This gives the following transcendental equation for the coupled eigenfrequency

$$\kappa L \tan \kappa L = \rho L \bigg/ \left[m\left(1 - \frac{\omega_n^2}{\omega^2}\right)\right] \quad \text{with} \quad \omega_n = \sqrt{\frac{k}{m}} \tag{14}$$

This equation is used to calculate the eigenfrequency in Section 4.

3. Numerical methods

3.1. Acoustic fluid equations

First, the movement of the piston is presumed to be known. Therefore the fluid flow in a tube with a moving end wall has to be calculated. In this section a numerical scheme for the linearised flow equations is presented. The acoustic equation (9) is then written in matrix form

$$\frac{\partial U}{\partial t} + A\frac{\partial U}{\partial x} = 0 \tag{15}$$

where

$$U = \begin{Bmatrix} \rho \\ \rho u \end{Bmatrix}, \qquad A = \begin{bmatrix} 0 & 1 \\ c_s^2 & 0 \end{bmatrix} \tag{16}$$

The domain is discretised into N nodes and N cells. The system (15) is discretised by the finite volume method. This gives the discretised equation for node i,

$$\frac{U_i^{n+1} - U_i^n}{\Delta t} + \frac{\Phi_{i+1/2}^* - \Phi_{i-1/2}^*}{\Delta x} = 0 \tag{17}$$

where $\Delta t = t^{n+1} - t^n$ denotes the time step and $\Delta x = x_{i+1/2} - x_{i-1/2}$ the cell size. The numerical flux Φ is calculated by the first order flux splitting upwind scheme,

$$\Phi_{i+1/2}^* = A^+ U_i^* + A^- U_{i+1}^* \tag{18}$$

where

$$A^+ \begin{bmatrix} c_s & 1 \\ c_s^2 & c_s \end{bmatrix}, \qquad A^- = \begin{bmatrix} -c_s & 1 \\ c_s^2 & -c_s \end{bmatrix} \tag{19}$$

The eigenvalues of A^+ are positive or zero and the eigenvalues of A^- are negative or zero. The scheme is explicit when the flux Φ^* in (18) is calculated with U^n and implicit when calculated with U^{n+1}. Implicit schemes allow for larger time steps than explicit schemes since their domain of stability is larger. In this case the implicit scheme is chosen since the solution at t^{n+1} is needed for the monolithical algorithm. The solution U_i^{n+1} is then calculated by

$$U_i^{n+1} + \frac{\Delta t}{\Delta x}(A^+U_i^{n+1} + A^-U_{i+1}^{n+1} - A^+U_{i-1}^{n+1} + A^-U_i^{n+1}) = U_i^n \tag{20}$$

The boundary conditions are taken into account by virtual nodes at the end points x_0 and x_{N+1}. With the variables at these nodes the fluxes $\Phi_{1/2}$ and $\Phi_{N+1/2}$ are calculated. The variables at the virtual nodes are calculated by linear extrapolation (see [20]). The boundary velocity is then imposed on the value at x_1 and x_N in the extrapolation equation. The extrapolated variable vector at x_0 is then calculated by

$$\boldsymbol{U}_0^{n+1} = \begin{Bmatrix} 2\boldsymbol{U}_1^{n+1}(1) & -\boldsymbol{U}_2^{n+1}(1) \\ & -\boldsymbol{U}_2^{n+1}(2) \end{Bmatrix} \tag{21}$$

The boundary condition at the moving piston is calculated by the so-called transpiration flux at $x_{N+1/2}$. This approach is only valid when the perturbations are small, which is a presumption of the acoustic theory (see (7)). A more general treatment on a moving domain is described in the next section for the nonlinear Euler equations. At x_{N+1} the variable vector is given by

$$\boldsymbol{U}_{N+1}^{n+1} = \begin{Bmatrix} 2\boldsymbol{U}_N^{n+1}(1) & -\boldsymbol{U}_{N-1}^{n+1}(1) \\ 2\bar{\rho}V* & -\boldsymbol{U}_{N-1}^{n+1}(2) \end{Bmatrix} \tag{22}$$

where $V*$ is the velocity of the piston, which is presumed to be known here. Eq. (20) has to be solved for the N nodes at every time step which gives a $2N \times 2N$ block tridiagonal system to solve. This system is solved by the block Thomas algorithm which is a generalisation of the Thomas algorithm [21].

3.2. *Euler fluid equations*

Next, the non-linear Euler equations are considered. For large deformations of the domain the computational mesh also has to be deformed. Although the movement of the piston is small in this case, the Euler equations are described on a general moving coordinate system to study the phenomenon.

On general moving coordinates the equations are described by the Arbitrary Lagrange Euler (ALE) method [22]. The coordinates are not moving with the particles (Lagrange) neither fixed to the laboratory (Euler) but can move in an arbitrary way. The one-dimensional integral ALE form of the Euler equations on a moving domain $\Omega(t)$ read

$$\frac{\partial}{\partial t}\int_{\Omega(t)} \boldsymbol{W}\,\mathrm{d}\Omega(t) + \int_{\Omega(t)} \frac{\partial \boldsymbol{F}}{\partial x}\,\mathrm{d}\Omega(t) = 0 \tag{23}$$

where the state vector $\boldsymbol{W}$ and the flux vector $\boldsymbol{F}$ are given by

$$\boldsymbol{W} = \begin{pmatrix} \rho \\ \rho u \\ \rho E \end{pmatrix} \quad \boldsymbol{F} = \begin{pmatrix} \rho U \\ \rho u U + p \\ \rho E U + up \end{pmatrix} \tag{24}$$

The contravariant velocity is defined by $U = u - w$. The coordinate velocity is denoted by w. Eq. (23) is closed by the equation of state for a perfect gas (2).

The domain is again subdivided into N nodes and N cells. Eq. (23) is discretised by means of the finite volume method. The discretised equations follow directly from (23) by dividing the domain into finite volumes and integrating over these volumes. The numerical equation for implicit time integration is given by

$$\mathcal{V}_i^{n+1}\boldsymbol{W}_i^{n+1} - \mathcal{V}_i^n\boldsymbol{W}_i^n = -\Delta t(\Phi(\boldsymbol{W}_i^{n+1}, \boldsymbol{W}_{i+1}^{n+1}) - \Phi(\boldsymbol{W}_i^{n+1}, \boldsymbol{W}_{i-1}^{n+1}))\,. \tag{25}$$

where $\mathcal{V}_i^n$ denotes the size of the ith cell at time $t = t^n$. $\boldsymbol{W}_i^n$ denotes the vector of conservative variables in node i at time $t = t^n$. Δt is the time step between t^n and t^{n+1}.

$\Phi(\boldsymbol{W}_i^{n+1}, \boldsymbol{W}_{i+1}^{n+1})$ is the numerical flux which is a numerical approximation of the flux $F(x_{i+1/2})$. The flux is discretised in an upwind fashion by the flux vector splitting of Van Leer [33]. The flux vector is split into two parts,

$$\Phi(\boldsymbol{W}_i^{n+1}, \boldsymbol{W}_{i+1}^{n+1}) = \Phi^+(\boldsymbol{W}_i^{n+1}) + \Phi^-(\boldsymbol{W}_{i+1}^{n+1}) \tag{26}$$

where the Jacobian of the flux vector Φ^+, $\partial\Phi^+/\partial\boldsymbol{W}$ is semi positive definite and the Jacobian of the flux vector Φ^-, $\partial\Phi^-/\partial\boldsymbol{W}$ is semi negative definite. The Van Leer flux on a moving coordinate system, which can be found in [7,23], is given by

$$\Phi^{\pm}(W_i) = \pm\frac{\rho}{4c}(U\pm c)^2\begin{pmatrix} 1 \\ \dfrac{\pm 2c - U}{\gamma} + u \\ \dfrac{-U^2 \pm 2Uc}{\gamma+1} + \dfrac{2c^2}{\gamma^2-1} + \dfrac{u^2}{2} - \dfrac{w(U\mp 2c)}{\gamma} \end{pmatrix} \tag{27}$$

where c is the local speed of sound defined by

$$c = \sqrt{\frac{\gamma p}{\rho}} \tag{28}$$

All flow variables are calculated at x_i except for the grid velocity which is calculated at $x_{i\pm 1/2}$ for $\Phi_{i\pm 1/2}$.

In order to calculate the numerical flux (26) at t^{n+1} the homogeneous property of the flux function $\boldsymbol{F}$, (24), is used

$$\boldsymbol{F} = \frac{\partial \boldsymbol{F}}{\partial \boldsymbol{W}}\boldsymbol{W} = \boldsymbol{J}\boldsymbol{W} \tag{29}$$

The numerical flux $\Phi^{n+1}_{i+1/2}$ is then written as

$$\begin{aligned}\Phi(\boldsymbol{W}_i^{n+1}, \boldsymbol{W}_{i+1}^{n+1}) &= \left.\frac{\partial \Phi^+}{\partial \boldsymbol{W}_i}\right|_{t^n} \boldsymbol{W}_i^{n+1} + \left.\frac{\partial \Phi^-}{\partial \boldsymbol{W}_{i+1}}\right|_{t^n} \boldsymbol{W}_{i+1}^{n+1} \\ &= \boldsymbol{J}^+\boldsymbol{W}_i^{n+1} + \boldsymbol{J}^-\boldsymbol{W}_{i+1}^{n+1}\end{aligned} \tag{30}$$

where $\boldsymbol{J}^+$ and $\boldsymbol{J}^-$ denote the Jacobian matrices of the Van Leer fluxes. The expressions for the flux derivatives are given in Appendix A. The numerical implicit scheme now reads

$$\mathcal{V}_i^{n+1}\boldsymbol{W}_i^{n+1} + \Delta t(\boldsymbol{J}^+\boldsymbol{W}_i^{n+1} + \boldsymbol{J}^-\boldsymbol{W}_{i+1}^{n+1} - \boldsymbol{J}^+\boldsymbol{W}_{i-1}^{n+1} - \boldsymbol{J}^-\boldsymbol{W}_i^{n+1}) = \mathcal{V}_i^n\boldsymbol{W}_i^n \tag{31}$$

where $\mathcal{V}_i^n$ is the size of the cell which belongs to node x_i. In order to solve (31) as a matrix equation the scheme is written with $\mathcal{V}\boldsymbol{W}$ as variables

$$(\mathcal{V}\boldsymbol{W})_i^{n+1} + \Delta t\left(\frac{\boldsymbol{J}^+ - \boldsymbol{J}^-}{\mathcal{V}_i^{n+1}}(\mathcal{V}\boldsymbol{W})_i^{n+1} + \frac{\boldsymbol{J}^-}{\mathcal{V}_{i+1}^{n+1}}(\mathcal{V}\boldsymbol{W})_{i+1}^{n+1} - \frac{\boldsymbol{J}^+}{\mathcal{V}_{i-1}^{n+1}}(\mathcal{V}\boldsymbol{W})_{i-1}^{n+1}\right) = (\mathcal{V}\boldsymbol{W})_i^n \tag{32}$$

The mesh is calculated as an equidistant distribution of the nodes over the tube length. When the mesh is moving the nodes remain equidistant. Therefore, the mesh velocity is calculated by a linear interpolation of the left (0) and right hand (V^*) velocities. The mesh points and mesh velocities for $i = 1, N$ are then calculated by

$$w_i^n = \frac{i-1}{N-1}V^* \quad\text{and}\quad x_i^n = x_i^n + \Delta t\, w_i^n \tag{33}$$

Next, the boundary conditions have to be imposed at the ends of the tube. As in the acoustic approach also virtual nodes are used to impose the boundary conditions. The conservative variables are linearly extrapolated from the interior. The boundary velocity is imposed at x_0 and x_N in the extrapolation equation. The extrapolated conservative variables at x_0 are calculated by

$$\begin{aligned}\boldsymbol{W}_0(1) &= 2\boldsymbol{W}_1(1) - \boldsymbol{W}_2(1) \\ \boldsymbol{W}_0(2) &= -\boldsymbol{W}_2(2) \\ \boldsymbol{W}_0(3) &= 2\boldsymbol{W}_1(3) - \boldsymbol{W}_2(3)\end{aligned} \tag{34}$$

At x_{N+1} the extrapolated variables are calculated by

$$\begin{aligned}\boldsymbol{W}_{N+1}(1) &= 2\boldsymbol{W}_N(1) - \boldsymbol{W}_{N-1}(1) \\ \boldsymbol{W}_{N+1}(2) &= 2\boldsymbol{W}_N(1)V^* - \boldsymbol{W}_{N-1}(2) \\ \boldsymbol{W}_{N+1}(3) &= 2\boldsymbol{W}_N(3) - \boldsymbol{W}_{N-1}(3)\end{aligned} \tag{35}$$

where the piston velocity V^* is used to extrapolate the second conservative variable ρu.

The implicit numerical scheme (31) has to be calculated for the N nodes at every time step. This gives a linear block tridiagonal system of size 3N × 3N. This system is solved again by the block Thomas algorithm.

3.3. Structure

In this section the numerical method for the time integration of the piston is discussed. Like in the previous section, the problem is presented as stand alone. The force which is exerted by the fluid on the structure is presumed to be known. The movement of the piston is described by the undamped equation of motion for a one degree of freedom system (4). This equation is numerically integrated in time by the constant average acceleration method. This is the optimal case of the Newmark method [24], i.e. the method has no numerical damping and is unconditionally stable.

First, the time domain is subdivided in discrete time steps denoted by Δt. Then, the assumption is made that the acceleration is constant in a time interval and equal to the mean of the beginning and the end of the interval,

$$\ddot{u}_s(\tau) = \frac{1}{2}(\ddot{u}_s^n + \ddot{u}_s^{n+1}) \tag{36}$$

where the parameter τ is defined by $\tau = t - t^n$. The velocity in the time interval is obtained by integrating (36) which gives

$$\dot{u}_s(\tau) = \dot{u}_s^n + \frac{1}{2}\tau(\ddot{u}_s^n + \ddot{u}_s^{n+1}) \tag{37}$$

Next, the displacement vector is obtained by integrating the velocity

$$u_s(\tau) = u_s^n + \tau\dot{u}_s^n + \frac{1}{4}\tau^2(\ddot{u}_s^n + \ddot{u}_s^{n+1}) \tag{38}$$

Then, the acceleration at time t^{n+1} is calculated by taking (38) at time t^{n+1}

$$\ddot{u}_s^{n+1} = \frac{4}{\Delta t^2}(u_s^{n+1} - u_s^n) - \frac{4}{\Delta t}\dot{u}_s^n - \ddot{u}_s^n \tag{39}$$

The velocity at time t^{n+1} is found with Eqs. (37) and (39), which gives

$$\dot{u}_s^{n+1} = \frac{2}{\Delta t}(u_s^{n+1} - u_s^n) - \dot{u}_s^n \tag{40}$$

In order to find the displacement vector at the new time level equations (38), (39) and (40) are substituted in the equation of motion (4) at time t^{n+1},

$$\left(\frac{4}{\Delta t^2}m + k\right)u_s^{n+1} = f^{n+1} + \frac{4}{\Delta t^2}mu_s^n + \frac{4}{\Delta t}m\dot{u}_s^n + m\ddot{u}_s^n \tag{41}$$

From this equation the displacement at time t^{n+1} is solved. Then, the acceleration and velocity are calculated by (39) and (40).

Next, the structural equations are written in the linear matrix form, which has to be solved every time step. The system is derived from Eqs. (39), (40) and (41). The system then reads

$$\begin{bmatrix} \frac{4}{\Delta t^2}m + k & 0 & 0 \\ -\frac{2}{\Delta t} & 1 & 0 \\ -\frac{4}{\Delta t^2} & 0 & 1 \end{bmatrix} \begin{Bmatrix} u_s^{n+1} \\ \dot{u}_s^{n+1} \\ \ddot{u}_s^{n+1} \end{Bmatrix} = \begin{bmatrix} \frac{4}{\Delta t^2}m & \frac{4}{\Delta t}m & m \\ -\frac{2}{\Delta t} & -1 & 0 \\ -\frac{4}{\Delta t^2} & -\frac{4}{\Delta t} & -1 \end{bmatrix} \begin{Bmatrix} u_s^n \\ \dot{u}_s^n \\ \ddot{u}_s^n \end{Bmatrix} + \begin{Bmatrix} f^{n+1} \\ 0 \\ 0 \end{Bmatrix} \tag{42}$$

It turns out that the system (42) is overdetermined which means that one line is superfluous. After some algebra it follows that

$$m\ddot{u}_s^n = -ku_s^n + f^n \tag{43}$$

This equation shows that the equilibrium equation (4) is satisfied at each time level. Elimination of the acceleration from (42) gives the reduced system

$$\begin{bmatrix} \frac{4}{\Delta t^2} m + k & 0 \\ -\frac{2}{\Delta t} & 1 \end{bmatrix} \begin{Bmatrix} u_s^{n+1} \\ \dot{u}_s^{n+1} \end{Bmatrix} = \begin{bmatrix} \frac{4}{\Delta t^2} m - k & \frac{4}{\Delta t} m \\ -\frac{2}{\Delta t} & -1 \end{bmatrix} \begin{Bmatrix} u_s^{n} \\ \dot{u}_s^{n} \end{Bmatrix} + \begin{Bmatrix} f^{n+1} + f^n \\ 0 \end{Bmatrix} \tag{44}$$

Eqs. (42) and (44) are used in the next section to integrate the structure in time.

3.4. *Fluid–structure coupling*

Now that the numerical methods for fluid and structure are described they have to be coupled. First, the staggered approach is described in Section 3.4.1. This method integrates the fluid and structure in time by two separate solvers. The interaction is taken into account by the boundary conditions at the fluid–structure interface. Then, the monolithical approach is derived in Section 3.4.2. Here, the fluid and structure are integrated in time as a single system where the interaction is also included.

3.4.1. *Staggered algorithm*

The staggered method is the most used method to solve the fluid–structure interaction problem in the time domain. Farhat [25] uses this method to calculate panel flutter. Similar test cases are studied by Piperno [7,26] and Blom and Leyland [9]. The flutter of airfoils with this method is studied by Rausch et al. [27], Prananta [3,4], Farhat and Lin [28], Piperno [7] and Blom and Leyland [8]. The piston problem, which is studied here, was also studied by Piperno [6,7] in order to investigate subcycling techniques on coupling algorithms.

The staggered method preserves the fluid and structure solvers as separate solvers. Both parts are alternately integrated in time. The interaction is taken into account by the boundary conditions of both solvers. As a consequence there exists a time lag between the integration of the fluid and structure. When the time steps are small the influence of the time lag can be neglected. Here, the influence of large time steps on the lagging error is investigated.

There are several possibilities for a staggered algorithm. Prananta and Hounjet [12] used structural as well as aerodynamical predictors in the algorithms. Bendiksen [15] used a coupling algorithm in the Runge–Kutta scheme where the interaction was updated also on intermediate time levels. A staggered scheme with a structural predictor is investigated here. The algorithm is schematically depicted in Fig. 2. At time $t = t^n$ the state of the fluid, structure and mesh are known. The next steps are taken to integrate the fluid–structure system from t^n to t^{n+1}:

(i) Predict the state of the structure at the end of the current time step ($t = t^{n+1}$).
(ii) Integrate the fluid to the next time level using the predicted state of the structure.
(iii) Update the structure to the next time level using the fluid pressures on the boundary.

REMARKS

(i) Two different predictions are applied to the problem. Prediction 1 is given by a zero order prediction

$$\{\dot{u}^{n+1}\} = \{\dot{u}^n\} \tag{45}$$

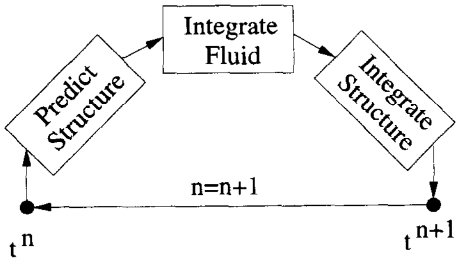

Fig. 2. Staggered coupling algorithm.

Prediction 2 is a first-order prediction according to

$$\{\dot{u}^{n+1}\} = \{\dot{u}^n\} + \Delta t\{\ddot{u}^n\} \tag{46}$$

(ii) The fluid is integrated by the acoustic or Euler algorithms of Sections 3.1 and 3.2, respectively.
(iii) The structure is updated by the algorithms described in Section 3.3.

The crucial part in this algorithm is the prediction of the structural state in step 1. The velocity in a time step has to correspond to the distance covered the same time step. The structural velocity is linear in time for the constant average acceleration method. Therefore, the covered distance is calculated exactly by trapezoidal integration of the velocity. The boundary velocity in the fluid solver has then to be calculated by

$$V^* = \frac{1}{2}(\dot{u}_s^{n+1} + \dot{u}_s^n) \tag{47}$$

The velocity $\dot{u}_s^{n+1}$ is calculated by the structural prediction (45) or (46). Taking prediction 2 gives a more precise approximation for $\dot{u}_s^{n+1}$, therefore it is expected to give better results.

3.4.2. Monolithical algorithm

In this section the monolithical time integration algorithm for fluid and structure is derived. Felker [29,30] constructed a monolithical solution algorithm for static fluid–structure interaction. He used Newton's algorithm to converge to static equilibrium between fluid and structure. Dynamic fluid–structure interaction contains an additional difficulty which is the time lag between fluid and structure which has to be avoided. Alonso and Jameson [17] circumvented this problem by updating the interaction every subiteration in their implicit algorithm. Melville et al. [18] and Morton et al. [19] used a similar approach. However, this algorithm also remains staggered.

Dynamic fluid–structure interaction involves time dependent information transfer from the fluid to the structure and vice versa. This information transfer only acts on the fluid–structure boundary. On the one hand, the fluid pressures are transferred to the structure via the external force which acts on the structure. On the other hand, the velocity of the mesh is equal to the velocity of the structure at the fluid–structure interface. In the staggered approach which is discussed in Section 3.4.1 this information transfer is not calculated at the same time. In the staggered approach a prediction of the structural velocity is transferred to the fluid. If this prediction were exact, there would be no extra energy transfer in the staggered algorithm [7]. In the monolithical approach the difference is zero by definition since the whole system is implicit including the interaction. The idea of a monolithical algorithm is schematically shown in Fig. 3. There is no time lag in the information transfer, since fluid and structure are enclosed in one system.

First, the monolithical algorithm is globally described in terms of matrix equations. After that the specific coupling terms in the equations are derived for the linear acoustic and nonlinear Euler solvers.

When the fluid is implicitly integrated a linear matrix equation has to be solved for every time step. This equation for the fluid is written as

$$[A_f]\{X_f^{n+1}\} = [B_f]\{X_f^n\} + \{F_f\} \tag{48}$$

where X_f is the vector which contains the fluid variables. The force term F_f contains the boundary condition at the moving piston, therefore it is a function of the structural velocity $\dot{u}_s$. The numerical scheme for the fluid is enclosed in the matrices A_f and B_f.

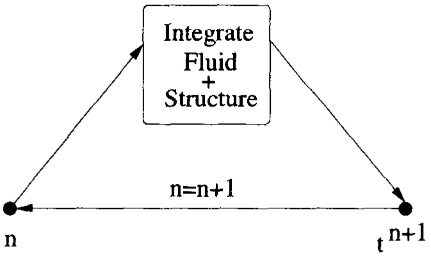

Fig. 3. Monolithical coupling algorithm.

The implicit integration of the structure involves the same type of matrix equation has to be solved for every time step. This equation is written as

$$[A_s]\{X_s^{n+1}\} = [B_s]\{X_s^n\} + \{F_s\} \tag{49}$$

where X_s is the vector with structure variables. The force term F_s is a function of the fluid pressure. The matrices A_s and B_s contain the numerical scheme for the structure.

Next, Eqs. (48) and (49) are written as one matrix system. The terms in the force functions F_f and F_s which are a function of X_s and X_f, respectively, are expressed in coupling matrices

$$\begin{bmatrix} [A_f] & [Ca_{sf}] \\ [Ca_{fs}] & [A_s] \end{bmatrix} \begin{Bmatrix} X_f^{n+1} \\ X_s^{n+1} \end{Bmatrix} = \begin{bmatrix} [B_f] & [Cb_{sf}] \\ [Cb_{fs}] & [B_s] \end{bmatrix} \begin{Bmatrix} X_f^n \\ X_s^n \end{Bmatrix} + \begin{Bmatrix} \bar{F}_f \\ \bar{F}_s \end{Bmatrix} \tag{50}$$

The coupling matrix Ca_{sf} contains the implicit boundary velocity term in the fluid equation. Ca_{fs} takes the implicit forcing term for the structure into account. The coupling matrices Cb_{sf} and Cb_{fs} are the explicit counterparts of the implicit Ca matrices. The force vectors $\bar{F}_f$ and $\bar{F}_s$ are the residual terms which are neither a function of the structure nor the fluid variables.

3.4.2.1. Acoustic equations. Next, the coupling terms for the acoustic equations are derived. The movement of the piston is taken into account by the virtual node. This relation is expressed in Eq. (22). The velocity of the piston V^* in this equation is incorporated in the matrix Ca_{sf} for implicit interaction and in Cb_{sf} for explicit interaction. Eq. (47) is verified exactly since the structural velocity at t^{n+1} is used in the calculation of the fluid. When (47) is substituted in Eq. (20) with the use of the virtual node (22), the fluid equation for node N reads

$$\begin{aligned} &\frac{\Delta t}{\Delta x}\left(\boldsymbol{A}^- \begin{Bmatrix} 2\boldsymbol{U}_N^{n+1}(1) - \boldsymbol{U}_{N-1}^{n+1}(1) \\ -\boldsymbol{U}_{N-1}^{n+1}(2) \end{Bmatrix} + \boldsymbol{A}^- \begin{Bmatrix} 0 \\ \bar{\rho}\dot{u}_s^{n+1} \end{Bmatrix}\right) + \boldsymbol{U}_N^{n+1} \\ &\quad + \frac{\Delta t}{\Delta x}(\boldsymbol{A}^+\boldsymbol{U}_N^{n+1} - \boldsymbol{A}^+\boldsymbol{U}_{N-1}^{n+1} + \boldsymbol{A}^-\boldsymbol{U}_N^{n+1}) = \boldsymbol{U}_N^n - \frac{\Delta t}{\Delta x}\boldsymbol{A}^- \begin{Bmatrix} 0 \\ \bar{\rho}\dot{u}_s^n \end{Bmatrix} \end{aligned} \tag{51}$$

This equation expresses the discretised fluid equations at node N. In terms of Eq. (50) this means that Ca_{sf} contains the terms in front of $\dot{u}_s^{n+1}$. The matrix Cb_{sf} is composed of the terms in front of $\dot{u}_s^n$ on the right-hand side of (51).

Eq. (44) is used to integrate the structure, since the fluid is described by two variables per node. In this way the complete matrix equation (50) is block tridiagonal where the blocks remain 2 × 2. The external force $f^{n+1} + f^n$ in this equation is equal to the pressure difference calculated by (5)

$$f^{n+1} + f^n = p^{n+1} + p^n - 2p_a = c_s^2(\rho_N^{n+1} + \rho_N^n) - 2p_a = c_s^2(\boldsymbol{U}_N^{n+1}(1) + \boldsymbol{U}_N^n(1)) - 2p_a \tag{52}$$

Next, the structural integration (44) is written as

$$\begin{aligned} &-\begin{bmatrix} c_s^2 & 0 \\ 0 & 0 \end{bmatrix} \begin{Bmatrix} \boldsymbol{U}_N^{n+1}(1) \\ \boldsymbol{U}_N^{n+1}(2) \end{Bmatrix} + \begin{bmatrix} \frac{4}{\Delta t^2}m + k & 0 \\ -\frac{2}{\Delta t} & 1 \end{bmatrix} \begin{Bmatrix} u_s^{n+1} \\ \dot{u}_s^{n+1} \end{Bmatrix} \\ &= \begin{bmatrix} \frac{4}{\Delta t^2}m - k & \frac{4}{\Delta t}m \\ -\frac{2}{\Delta t} & -1 \end{bmatrix} \begin{Bmatrix} u_s^n \\ \dot{u}_s^n \end{Bmatrix} + \begin{bmatrix} c_s^2 & 0 \\ 0 & 0 \end{bmatrix} \begin{Bmatrix} \boldsymbol{U}_N^n(1) \\ \boldsymbol{U}_N^n(2) \end{Bmatrix} - \begin{Bmatrix} 2p_a \\ 0 \end{Bmatrix} \end{aligned} \tag{53}$$

This equation is then fitted into the last two lines of (50). Hence the matrix Ca_{fs} of (50) is given by the first matrix of (53). Cb_{fs} contains the matrix in front of U_N^n on the right-hand side of (53). $\bar{F}_s$ is given by the last vector of (53).

3.4.2.2. Euler equations. Next the coupling matrices for the Euler equations are specified. These coupling matrices are more complicated to calculate. However, the consideration remains conceptually the same as for the acoustic equations. The velocity of the piston is taken into account by the virtual node, (35). Like in the acoustic algorithm the consistent piston velocity (47) is used in the calculation of the virtual node. When (47) is substituted into (35) and used in (32) for the fluid equation at node N this equation reads

$$\begin{aligned} &\Delta t \frac{\boldsymbol{J}^-}{\mathcal{V}_{N+1}^{n+1}} \begin{Bmatrix} 2(\mathcal{V}\boldsymbol{W})_N^{n+1}(1) - (\mathcal{V}\boldsymbol{W})_{N-1}^{n+1}(1) \\ - (\mathcal{V}\boldsymbol{W})_{N-1}^{n+1}(2) \\ 2(\mathcal{V}\boldsymbol{W})_N^{n+1}(3) - (\mathcal{V}\boldsymbol{W})_{N-1}^{n+1}(3) \end{Bmatrix} + \Delta t \frac{\boldsymbol{J}^-}{\mathcal{V}_{N+1}^{n+1}} \begin{Bmatrix} 0 \\ (\mathcal{V}\boldsymbol{W})_N^n(1)\dot{u}_s^{n+1} \\ 0 \end{Bmatrix} \\ &+ (\mathcal{V}\boldsymbol{W})_N^{n+1} + \Delta t \left(\frac{\boldsymbol{J}^+ - \boldsymbol{J}^-}{\mathcal{V}_N^{n+1}} (\mathcal{V}\boldsymbol{W})_N^{n+1} - \frac{\boldsymbol{J}^+}{\mathcal{V}_{N-1}^{n+1}} (\mathcal{V}\boldsymbol{W})_{N-1}^{n+1} \right) \\ &= (\mathcal{V}\boldsymbol{W})_N^n - \Delta t \frac{\boldsymbol{J}^-}{\mathcal{V}_{N+1}^{n+1}} \begin{Bmatrix} 0 \\ (\mathcal{V}\boldsymbol{W})_N^n(1)\dot{u}_s \\ 0 \end{Bmatrix} \end{aligned} \tag{54}$$

This equation is fitted into the last three lines of (50). The matrix Ca_{sf} contains the left-hand side multiplication terms in front of $\dot{u}_s^{n+1}$ in (54). The matrix Cb_{sf} consists of the terms in front of $\dot{u}_s^n$ on the right-hand side of (54).

For the integration of (32) the cell size $\mathcal{V}^{n+1}$ at time t^{n+1} is needed. This value is not known at time t^{n+1}. Therefore, it is calculated as a linear extrapolation from the current and previous time level according to

$$\mathcal{V}^{n+1} = 2\mathcal{V}^n - \mathcal{V}^{n-1} \tag{55}$$

The term Ca_{fs} in the matrix represents the pressure at t^{n+1}. This pressure has to be calculated by a Taylor expansion as it is not an explicit variable

$$p^{n+1} = p^n + \left.\frac{\partial p}{\partial \boldsymbol{W}}\right|_{t^n} \Delta \boldsymbol{W} \tag{56}$$

where

$$\begin{aligned} \frac{\partial p^n}{\partial \boldsymbol{W}(1)} &= (\gamma - 1)\frac{u^2}{2} \\ \frac{\partial p^n}{\partial \boldsymbol{W}(2)} &= (1 - \gamma)u \\ \frac{\partial p^n}{\partial \boldsymbol{W}(3)} &= \gamma - 1 \end{aligned} \tag{57}$$

It is easily verified that the pressure also satisfies the homogeneous property. Therefore, the pressure at t^{n+1} is calculated as

$$p^{n+1} = \left.\frac{\partial p}{\partial \boldsymbol{W}}\right|_{t^n} \boldsymbol{W}^{n+1} \tag{58}$$

Eq. (42) is used to integrate the structure as the Euler equations describe the fluid with three variables per node. In this way the matrix structure of (50) remains block tridiagonal with block size 3 × 3. Eq. (56) is then substituted in Eq. (42) which gives

$$\begin{aligned} &-\begin{bmatrix} (\gamma-1)\dfrac{(u^n)^2}{2} & (1-\gamma)u^n & \gamma-1 \\ 0 & 0 & 0 \\ 0 & 0 & 0 \end{bmatrix} \begin{Bmatrix} \boldsymbol{W}_N^{n+1}(1) \\ \boldsymbol{W}_N^{n+1}(2) \\ \boldsymbol{W}_N^{n+1}(3) \end{Bmatrix} + \begin{bmatrix} \dfrac{4}{\Delta t^2} m + k & 0 & 0 \\ -\dfrac{2}{\Delta t} & 1 & 0 \\ -\dfrac{4}{\Delta t^2} & 0 & 1 \end{bmatrix} \begin{Bmatrix} u_s^{n+1} \\ \dot{u}_s^{n+1} \\ \ddot{u}_s^{n+1} \end{Bmatrix} \\ &= \begin{bmatrix} \dfrac{4}{\Delta t^2} m & \dfrac{4}{\Delta t} & m \\ -\dfrac{2}{\Delta t} & -1 & 0 \\ -\dfrac{4}{\Delta t^2} & -\dfrac{4}{\Delta t} & -1 \end{bmatrix} \begin{Bmatrix} u_s^n \\ \dot{u}_s^n \\ \ddot{u}_s^n \end{Bmatrix} - \begin{Bmatrix} p_a \\ 0 \\ 0 \end{Bmatrix} \end{aligned} \tag{59}$$

This equation forms the last three lines of the total fluid–structure interaction system (50). Accordingly, the matrix Ca_{fs} in (50) is given by the first matrix of (59). The matrix Cb_{fs} is empty in this case and $\bar{F}_{\mathrm{s}}$ is given by the last vector of (59).

Finally also, the movement of the mesh is taken into account. Then, the mesh velocity also becomes an unknown in the fluid equations since it is a function of u_{s}^{n+1}. The interval of the mesh velocity $\Delta w = w^{n+1} - w^n$ is added to the vector of conservative variables $\boldsymbol{W}$. The partial derivatives of the flux to the mesh velocity also have to be taken into account as the flux $\Phi^{\pm}$ is a function of w. The flux at t^{n+1} is calculated by

$$\boldsymbol{F}^{n+1} = \boldsymbol{F}^n + \frac{\partial \boldsymbol{F}}{\partial \boldsymbol{W}} \Delta \boldsymbol{W} + \frac{\partial \boldsymbol{F}}{\partial w} \Delta w = \boldsymbol{F}^n + \boldsymbol{J}\, \Delta \boldsymbol{W} + \frac{1}{2} \frac{\partial \boldsymbol{F}}{\partial w} \Delta w \tag{60}$$

Making use of the homogeneous property this is written as

$$\boldsymbol{F}^{n+1} = \boldsymbol{J} \boldsymbol{W}^{n+1} + \frac{1}{2} \frac{\partial \boldsymbol{F}}{\partial w} \Delta w \tag{61}$$

The factor $\frac{1}{2}$ is added because of the Geometrical Conservation Law (GCL, [31,32]). This law states that a uniform flow has to be a solution of the discretised flow equations on a moving mesh. Therefore, the fluxes which calculate the transpiration of the conservative quantities through the moving mesh have to be calculated consistently with the discretisation [25]. In this case the mesh velocity w is a linear function in time between the different time levels, since it follows the structural motion. Accordingly, the transpiration fluxes have to be calculated by the trapezoidal rule. This means it has to be calculated at $t^{n+1/2}$. The flux at $w(t^{n+1/2})$ is then calculated by

$$\boldsymbol{F}(w(t^{n+1/2})) = \boldsymbol{F}^n + \frac{1}{2} \frac{\partial \boldsymbol{F}}{\partial w} \Delta w \tag{62}$$

The numerical flux at $x_{i+1/2}$ is given by

$$\Phi_{i+1/2} = \Phi^+(\boldsymbol{W}_i, w_{i+1/2}) + \Phi^-(\boldsymbol{W}_{i+1}, w_{i+1/2}) \tag{63}$$

where $w_{i+1/2} = \frac{1}{2}(w_i + w_{i+1})$. For the calculation of the numerical flux at t^{n+1} the partial derivatives of these fluxes with respect to the mesh velocities w are needed. It can be verified that these derivatives satisfy the following property

$$\frac{\partial \Phi^*\left(\frac{1}{2} w\right)}{\partial w} = \frac{1}{2} \frac{\partial \Phi^*(w)}{\partial w} \tag{64}$$

The numerical representation of (62) is then given by

$$\Phi_{i+1/2}^{n+1} = \Phi_{i+1/2}^{n} + \frac{1}{4}\left[\frac{\partial \Phi^+(\boldsymbol{W}_{i,w_{i+1/2}})}{\partial w} + \frac{\partial \Phi^-(\boldsymbol{W}_{i+1,w_{i+1/2}})}{\partial w}\right](\Delta w_i + \Delta w_{i+1}) \tag{65}$$

The partial derivatives of the numerical fluxes with respect to the mesh velocity w are given in Appendix B.

The velocities of the mesh become a function of the velocities of the neighbouring mesh velocities. This adds a fourth equation to the discretised Euler equations (31). This equation expresses the spatial distribution of the mesh movement (33), at time t^{n+1} which reads

$$w_i^{n+1} - \frac{x_i}{x_{i+1}} w_{i+1}^{n+1} = 0 \tag{66}$$

This is now written as a linear function of the variable Δw to be compatible with the variable introduced in (65)

$$\Delta w_i^{n+1} - \frac{x_i}{x_{i+1}} \Delta w_{i+1}^{n+1} = \frac{x_i}{x_{i+1}} w_{i+1}^n - w_i^n \tag{67}$$

As Eq. (66) is satisfied at all times starting at $t = t_{\mathrm{begin}}$, the right-hand side of Eq. (67) is zero by induction. At the piston the velocity of the mesh at time t^{n+1} has to be equal to the piston velocity. Therefore, the expression for the mesh velocity as function of Δw_N is

$$\Delta w_N^{n+1} - \dot{u}_s^{n+1} = -w_N^n \tag{68}$$

This is also a boundary condition of the fluid which is a function of $\dot{u}_s^{n+1}$. Therefore, (68) modifies Ca_{sf} and B_f. The structure of the linear system (50) is not affected by the addition of the mesh, structure and interaction. The matrix remains block tridiagonal with blocks of 4 × 4.

4. Numerical results

The numerical methods are now validated on a documented piston problem. The numerical values of the parameters are chosen the same as in the thesis of Piperno [7], which were designed for strong coupling effects. They are listed in Table 1. The first eigenfrequency of the coupled system is calculated by the transcendental equation (14). The solution of this equation gives a numerical value of 341.61 rad/s. The eigenfrequency is considerably larger compared to the structural eigenfrequency (100 rad/s). The eigenfrequency of the fluid closed in a tube with two fixed ends is calculated from (14) by taking the limit $m \rightarrow \infty$. This gives an eigenfrequency of $\omega_f = \pi c_s / L = 1030.96$ rad/s. This is much larger than the coupled eigenfrequency of the system, which shows the strong coupling effects of these parameters.

4.1. Acoustic results

First, the problem is solved by means of the acoustic solver which is described in Section 3.1. The fluid domain is discretised with 100 nodes. The initial conditions for the piston are taken as $u_s = 0$ and $\dot{u}_s = 20$ m/s.

The comparison of the piston frequencies for the three coupling algorithms and different CFL numbers is shown in Table 2. At CFL = 1 all algorithms predict the correct frequency. As the CFL number is increased, the monolithical algorithm performs better than the staggered ones. The prediction 2 algorithm gives better results than prediction 1. This confirms the expectations argued at the end of Section 3.4.1.

The amplitude of the piston is depicted in Fig. 4 for the three algorithms at CFL = 1. There is not much difference between the solutions. The prediction 2 curve is a little more damped than the prediction 1 curve. In turn the monolithical algorithm shows more damping than both staggered algorithms.

The differences between the different algorithms is more pronounced when the CFL number increases. The amplitude of the piston calculated with prediction 1 staggered algorithm for higher CFL numbers is depicted in Fig. 5. The results with prediction 2 are shown in Fig. 6. The damping of the signal is caused by the numerical damping in the fluid solver since the structure solver has no numerical damping. One can see that the numerical damping is higher for the prediction 2 solution. The piston has to vibrate around the equilibrium position as there is no external force which acts on the structure. As the CFL number increases the deviation of the solution to the equilibrium position is also increasing. This deviation is larger for the prediction 1 solution caused by the less accurate prediction.

Table 1. Parameters for piston problem

L	1	m
$\bar{\rho}$	1.3	kg
c_s	328.17	m/s
p_a	1×10^5	Pa
ω_n	100	rad/s
m	0.8	kg
γ	1.4	

Table 2. Comparison of piston frequencies (rad/s), acoustic

	CFL = 1	CFL = 10	CFL = 30	CFL = 50
Prediction 1	341.6	342.2	346.9	357.4
Prediction 2	341.6	342.2	346.7	347.5
Monolithical	341.6	341.5	340.9	339.9

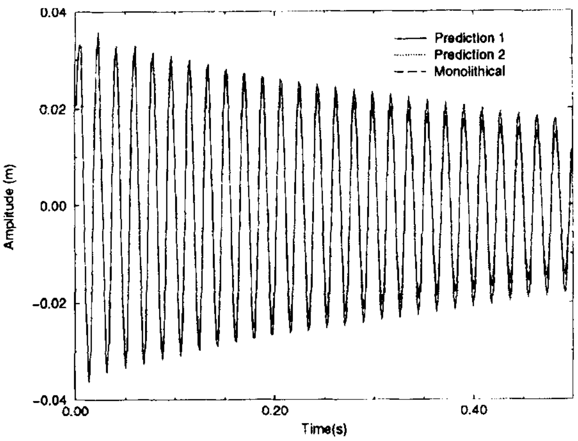

Fig. 4. Amplitude of piston, CFL = 1, acoustic.

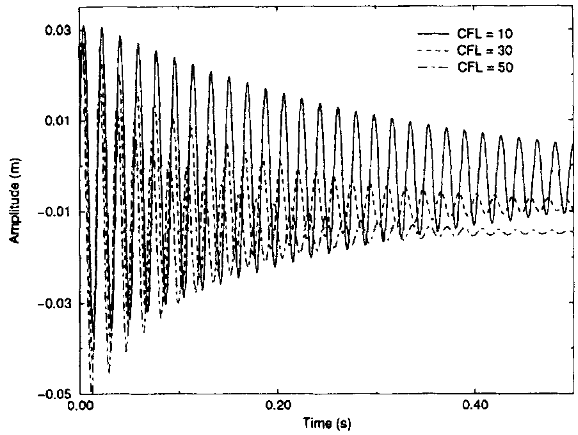

Fig. 5. Amplitude of piston, acoustic-staggered algorithm, prediction 1.

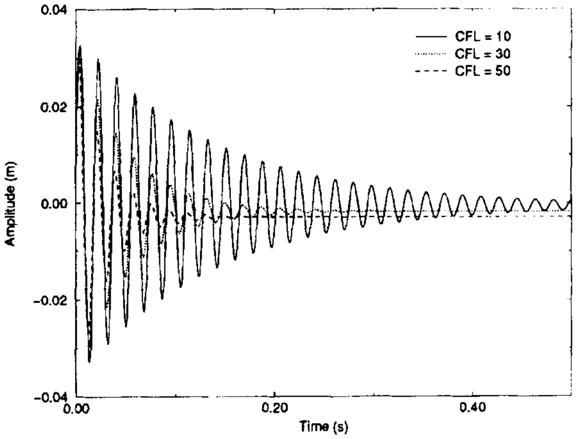

Fig. 6. Amplitude of piston, acoustic-staggered algorithm, prediction 2.

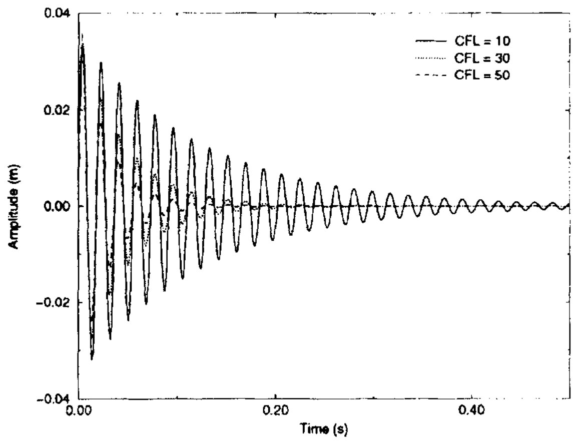

Fig. 7. Amplitude of piston, acoustic-monolithical algorithm.

The problem is then solved by the monolithical algorithm. The oscillation of the piston is shown in Fig. 7. The amplitude is more damped than the prediction 2 solution. Furthermore, the solution oscillates perfectly around the equilibrium position.

4.2. Stability

Next, the stability of the coupling schemes is investigated. The fluid–structure algorithm is written as a matrix vector equation, as in Eq. (50). This equation is then written as

$$[A]\{X^{n+1}\} = [B]\{X^n\} + \{F\} \tag{69}$$

where

$$[A] = \begin{bmatrix} [A_\mathrm{f}] & [Ca_\mathrm{sf}] \\ [Ca_\mathrm{fs}] & [A_\mathrm{s}] \end{bmatrix} \qquad [B] = \begin{bmatrix} [B_\mathrm{f}] & [Cb_\mathrm{sf}] \\ [Cb_\mathrm{fs}] & [B_\mathrm{s}] \end{bmatrix} \tag{70}$$

$$\{X^{n+1}\} = \begin{Bmatrix} X_\mathrm{f}^{n+1} \\ X_\mathrm{s}^{n+1} \end{Bmatrix} \qquad \{X^n\} = \begin{Bmatrix} X_\mathrm{f}^n \\ X_\mathrm{s}^n \end{Bmatrix} \qquad \{F\} = \begin{Bmatrix} F_\mathrm{f} \\ \bar{F}_\mathrm{s} \end{Bmatrix} \tag{71}$$

The stability of the scheme (69) is determined by the spectral radius of the matrix

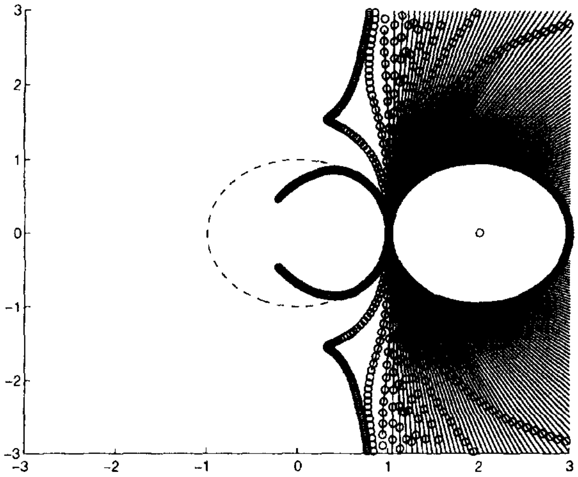

Fig. 8. Eigenvalue trajectories for staggered algorithm, prediction 1, CFL 1-200, ΔCFL = 2.

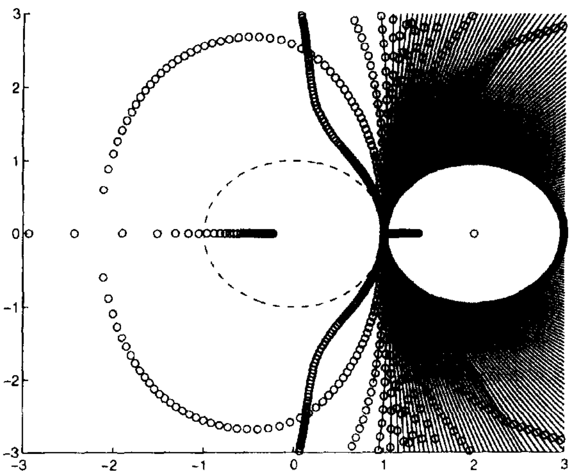

Fig. 9. Eigenvalue trajectories for staggered algorithm, prediction 2, CFL 1-200, ΔCFL = 2.

$$[C] = [B]^{-1}[A] \tag{72}$$

Stability of the system is guaranteed when the spectral radius of the matrix $[C]$ is larger than one. The trajectories of the spectral radii for the different coupling algorithms are depicted in Figs. 8–10 in the complex plane. At CFL = 1 all eigenvalues are roughly situated at a circle of radius one centred at $(2,0)$, plus one eigenvalue in the centre of this circle. The eigenvalues follow the solid lines as the CFL increases. The small circles mark the eigenvalues at CFL intervals of 2 for the staggered schemes and 20 for the monolithical scheme. The dashed line depicts the unit circle which is the limit of stability. One can see that the staggered algorithms are conditionally stable. The staggered scheme with prediction 1 becomes unstable at CFL = 80. The stability limit of the prediction 2 algorithm is CFL = 136. The monolithical scheme however, does not become unstable. For this scheme the smallest eigenvalue approaches $(-1,0)$ when the CFL is further increased but never reaches this limit.

Next, the fluid flow in the tube is calculated by the Euler equations. The initial conditions and number of nodes are taken the same as for the acoustic case. Here the staggered scheme only uses prediction 2 since it showed superior results for the acoustic simulations. The piston frequencies are compared in Table 3 for the different coupling algorithms and different CFL numbers. Here again, the results are very similar for small CFL numbers. The frequencies are better predicted with the staggered algorithm than with the monolithical algorithm.

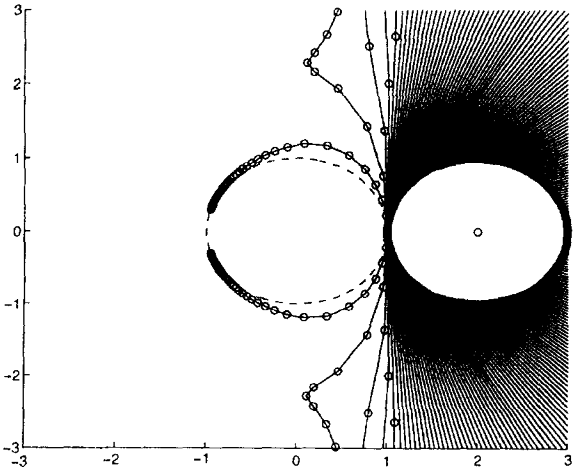

Fig. 10. Eigenvalue trajectories for monolithical algorithm, CFL 1-1000, ΔCFL = 20.

Table 3. Comparison of piston frequencies (rad/s), Euler

	CFL = 1	CFL = 10	CFL = 30	CFL = 50
Prediction 2	341.6	341.9	343.4	346.2
Monolithical	341.7	343.1	350.4	368.0

This is probably caused by linearisation errors for the pressure (58), and extrapolation of the area (55). The amplitude of the piston is depicted in Fig. 11 for both algorithms at CFL = 1. The results are very similar. The monolithical scheme shows more damping than the staggered scheme.

More differences occur when the CFL number is increased. The amplitude of the piston calculated with the staggered scheme is depicted in Fig. 12 for several CFL numbers. The results are similar to the acoustic results. For the staggered scheme the solution deviates more and more from the equilibrium position as the CFL number increases.

The amplitude of the calculation with the monolithical algorithm is depicted in Fig. 13. This solution is again more damped than the staggered solution. The monolithical scheme shows no non-physical deviation from the equilibrium position.

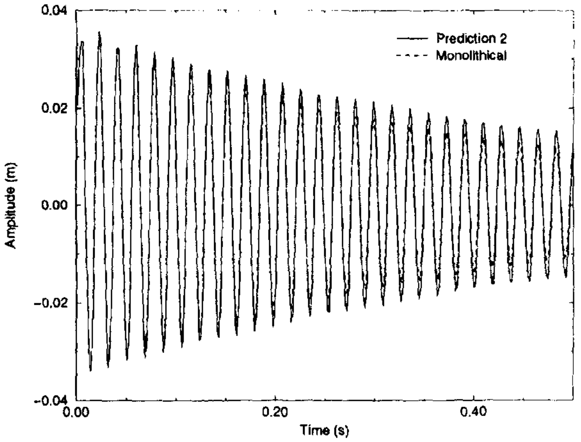

Fig. 11. Amplitude of piston, CFL = 1, Euler.

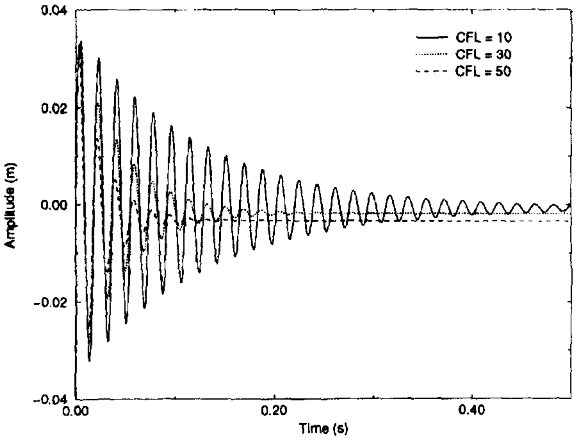

Fig. 12. Amplitude of piston, Euler-staggered algorithm.

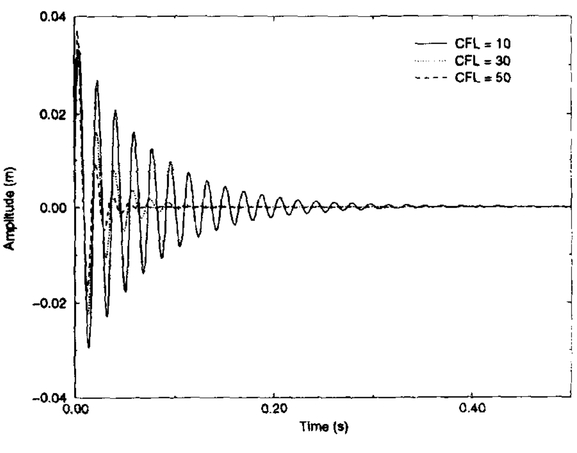

Fig. 13. Amplitude of piston, Euler-monolithical algorithm.

4.4. Analysis of damping

The numerical damping of the algorithms is analysed in some more detail now. Figs. 5–7 show that the numerical damping is higher when the prediction is more exact. Hence, the highest damping occurs in the monolithical algorithm and the prediction 2 solution is more damped than that of prediction 1. This observation is analysed in this section.

The energy which is transferred from the fluid to the structure per period is calculated by the integral of the product of the structural velocity and force which acts upon the structure

$$E = \int_0^T \dot{u}_s(t) f(t)\,\mathrm{d}t \tag{73}$$

In the analytical case this energy has to be zero as there is no production or dissipation in the physical system. Numerically, the energy decreases since there exists numerical dissipation in the fluid solver. To calculate the energy, pressure and velocity have to be known as a function of time.

From a quasi-steady consideration on the piston problem it follows that the force and displacement of the piston have to be 180° out of phase (when the piston moves to the right the pressure has to decrease). Hence, the analytical force and displacement are chosen as

$$\begin{aligned} f(t) &= \bar{f}\cos(\omega t) \\ u_s(t) &= -\bar{u}_s\cos(\omega t) \end{aligned} \tag{74}$$

where $\bar{f}$ is the force amplitude and $\bar{u}_s$ is the amplitude of the displacement. The velocity of the piston is then calculated by taking the partial derivative of the displacement to the time

$$\dot{u}_s = \omega\bar{u}_s\sin(\omega t) \tag{75}$$

The phase relationship of the force and velocity is confirmed by the calculation. The velocity and force are plotted as a function of time in Fig. 14. The force is divided by 200 to obtain a comparable amplitude in the figure. The calculation is performed with the monolithical scheme at CFL = 10. The 90° phase difference is clearly visible.

Now, the analytical transferred energy is calculated by the substitution of (74) and (75) in (73) which gives

$$E = \int_0^T \omega\bar{u}_s\sin(\omega t)\bar{f}\cos(\omega t)\,\mathrm{d}t = 0 \tag{76}$$

This shows that in the analytical case there is no net energy transfer between fluid and structure.

In the staggered case there exists a time lag between fluid and structure. This time lag is present in the prediction of the structure velocity which is used to calculate the pressure. So the pressure, which has the same

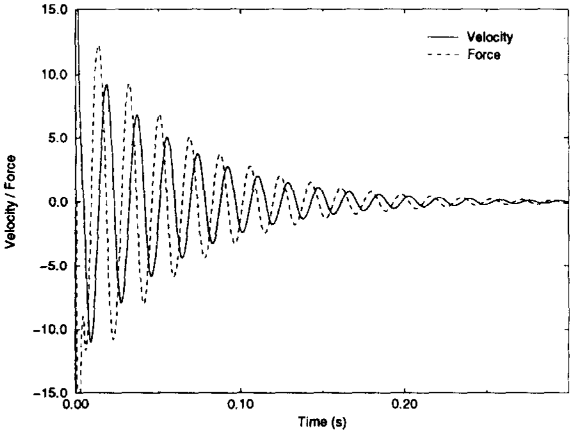

Fig. 14. Velocity and force/200, monolithical algorithm, CFL = 10.

time dependence as the force, is calculated at $t^{n+1} - \phi\,\Delta t$, where $0 \leq \phi < 1$ for the staggered schemes. Then, the energy is calculated by

$$\begin{aligned} E &= \int_0^T \omega \bar{u}_s \sin(\omega t) \bar{f} \cos(\omega(t - \phi\,\Delta t))\,\mathrm{d}t \\ &= \omega \bar{u}_s \bar{f} \int_0^T \sin(\omega t)(\cos(\omega t)\cos(\omega\phi\,\Delta t) + \sin(\omega t)\sin(\omega\phi\,\Delta t))\,\mathrm{d}t \\ &= \pi \bar{u}_s \bar{f} \sin(\omega\phi\,\Delta t) \end{aligned} \tag{77}$$

This calculation shows that there is an energy source which transfers energy from the fluid to the structure when the pressure is calculated too early. This term is scaled by $\sin(\omega\phi\,\Delta t)$ which is very small when the prediction is good or when the time steps are small.

The predictions 1 and 2 in the staggered scheme produce energy which is transferred to the structure. The numerical damping in the fluid solver compensates this production so that the final solution is still damped. The total damping depends on the sum of the numerical production and damping. This contributes to explain why the staggered scheme becomes unstable at high CFL numbers as shown in Section 4.2. The numerical energy production is in that case higher than the numerical dissipation.

It is concluded that in order to avoid energy creation and non-physical deviation a numerical time marching fluid–structure interaction algorithm has to satisfy the Interaction Consistency Law. This law is defined as

Interaction Consistency Law (ICL)

The time dependence of the boundary conditions for fluid and structure solvers has to be consistent with the discrete time integration of the structure and fluid solvers, respectively.

For the structure solver (constant average acceleration) this means that the external force $f(t)$ has to be calculated with the pressure at t^{n+1}, as shown in Section 3.3. The boundary velocity for the fluid solver has to be calculated with Eq. (47), as derived in Section 3.4.1. This velocity contains the structural velocity at t^{n+1}. Accordingly, the boundary conditions of fluid and structure both contain the implicit variables of structure and fluid respectively. Therefore, only the monolithical scheme satisfies the ICL. When a staggered scheme is used, prediction 2 is recommended. For other structure integration rules than the trapezoidal rule, another consistent boundary velocity, like (47), has to be derived.

The Interaction Consistency Law is not to be confused with the Geometrical Conservation Law. The GCL dictates the consistency of the mesh movement and fluid solver, whereas the ICL dictates the consistency of the boundary conditions and fluid/structure solvers.

The observed non-physical deviation of the piston can also be explained by the energy analysis. According to the first law of thermodynamics, total energy needs to be conserved. This is also the case for the piston problem. The energy which is created by the staggered scheme is stored in potential energy of the system. The non-physical deviation is negative, so energy is stored in an augmented pressure in the tube. Energy is also stored in the spring which is under tension at the end of the simulation.

5. Concluding remarks

A numerical analysis of different time marching fluid–structure interaction algorithms is presented. The relatively simple piston problem is chosen in order to concentrate on the coupling algorithms. The one-dimensional fluid is modelled by linear acoustic and nonlinear Euler equations. The acoustic equation is discretised by a first order upwind method. The nonlinear Euler equations are written in moving mesh coordinates by the Arbitrary Lagrange Euler method (ALE). These equations are discretised by the Van Leer scheme and integrated in time by an implicit method. The structure is integrated in time by the constant average acceleration method. In order to couple fluid and structure solvers first the staggered coupling method is adopted which integrates both mediums in time by separated solvers. The interaction is then taken into account by the boundary conditions. The method suffers from a time lag between the integration of fluid and structure. The influence of the time lag is studied by comparing two different predictions of the structure. Then, the novel monolithical algorithm is presented. Here, fluid and structure are integrated in time as one system. The time lag is not present in this algorithm. For the Euler equations the mesh movement is also implicitly coupled to the structure.

The acoustic calculations show that the staggered as well as the monolithical scheme converge to the analytical solution as the time step diminishes. The differences become more pronounced as the CFL number increases. The staggered schemes show a non-physical deviation from the mean position of the piston with increasing CFL. This deviation is diminished by an improvement of the structural prediction. The deviation is not present in the monolithical simulations. Stability analysis shows the unconditional stability of the monolithical scheme whereas the staggered schemes have a limited domain of stability. The domain of stability for the staggered scheme is enlarged when the prediction is improved. The calculations with the monolithical scheme show more damping than those with the staggered scheme. Analysis of the numerical damping shows that there is production of energy in the staggered algorithm since the prediction of the structure is not correct. The production of energy is diminished by the improved prediction. The results with nonlinear Euler equations show similar results. These simulations show the concept and feasibility of a monolithical time marching fluid–structure interaction scheme with nonlinear fluid equations on moving meshes. For a practical problem there are multiple dimensions involved. In n dimensions the fluid solver is modified by the addition of n mesh velocities to the number of variables and equations per node. For the Euler or Navier–Stokes equations in two dimensions this means that there are 6 variables per node and in three dimensions there are 8 variables per node. The discretisation of a multiple dimensional structure by many degrees of freedom can be reduced to several one degree of freedom problems by modal decomposition. These problems can be solved by the same technique as discussed in this paper. The present analysis leads to the definition of the Interaction Consistency Law (ICL). This law states that the time dependence of the boundary conditions for fluid and structure solvers has to be consistent with the time integration of the structure and fluid solvers, respectively. When this law is satisfied by the algorithm non-physical deviation and numerical energy production are avoided.

Acknowledgments

The author would like to thank Pénélope Leyland for her corrections and discussions on this paper. Financial support for this project was provided by the Leonhard Euler Center, the Swiss Pilot Center of the European Research Community On Flow Turbulence And Combustion (ERCOFTAC).

Appendix A. Jacobian matrices of the Van Leer fluxes

To calculate the derivatives of (27) this equation is first written as

$$\Phi^{\pm}(\mathbf{W}_i^n) = f_1^{\pm} f_2^{\pm} \begin{pmatrix} 1 \\ f_3^{\pm} \\ f_{41}^{\pm} + f_{42} + f_{43} + f_{44}^{\pm} \end{pmatrix} \tag{A.1}$$

where

$$\begin{aligned} f_1^{\pm} &= \pm \frac{\rho}{4c} \\ f_2^{\pm} &= (U \pm c)^2 \\ f_3^{\pm} &= \frac{\pm 2c - U}{\gamma} + u \\ f_{41}^{\pm} &= \frac{-U^2 \pm 2Uc}{\gamma + 1} \end{aligned} \tag{A.2}$$

$$
\begin{aligned}
f_{42} &= \frac{2c^2}{\gamma^2 - 1} \\
f_{43} &= \frac{u^2}{2} \\
f_{44}^{\pm} &= -\frac{w(U \mp 2c)}{\gamma}
\end{aligned}
$$

Now, the flux Jacobians are written as

$$
\begin{aligned}
\frac{\partial \Phi_1^{\pm}}{\partial \boldsymbol{W}_{123}} &= \frac{\partial f_1^{\pm}}{\partial \boldsymbol{W}_{123}} f_2^{\pm} + \frac{\partial f_2^{\pm}}{\partial \boldsymbol{W}_{123}} f_1^{\pm} \\
\frac{\partial \Phi_2^{\pm}}{\partial \boldsymbol{W}_{123}} &= \frac{\partial \Phi_1^{\pm}}{\partial \boldsymbol{W}_{123}} f_3^{\pm} + \frac{\partial f_3^{\pm}}{\partial \boldsymbol{W}_{123}} \Phi_1^{\pm} \\
\frac{\partial \Phi_3^{\pm}}{\partial \boldsymbol{W}_{123}} &= \frac{\partial \Phi_1^{\pm}}{\partial \boldsymbol{W}_{123}} f_4^{\pm} + \frac{\partial f_4^{\pm}}{\partial \boldsymbol{W}_{123}} \Phi_1^{\pm}
\end{aligned}
\tag{A.3}
$$

where $f_4^{\pm} = f_{41}^{\pm} + f_{42} + f_{43} + f_{44}^{\pm}$. Next, the partial derivatives are calculated. For $f_1^{\pm}$ they read

$$
\begin{aligned}
\frac{\partial f_1^{\pm}}{\partial \boldsymbol{W}_1} &= \pm\left(\frac{1}{4c} - \frac{\gamma(\gamma-1)(u^2 - E)}{8c^3}\right) \\
\frac{\partial f_1^{\pm}}{\partial \boldsymbol{W}_2} &= \pm\left(\frac{\gamma(\gamma-1)u}{8c^3}\right) \\
\frac{\partial f_1^{\pm}}{\partial \boldsymbol{W}_3} &= \mp\left(\frac{\gamma(\gamma-1)}{8c^2}\right)
\end{aligned}
\tag{A.4}
$$

For $f_2^{\pm}$

$$
\begin{aligned}
\frac{\partial f_2^{\pm}}{\partial \boldsymbol{W}_1} &= 2(U \pm c)\left(-\frac{u}{\rho} \pm \frac{\gamma(\gamma-1)(u^2 - E)}{2\rho c}\right) \\
\frac{\partial f_2^{\pm}}{\partial \boldsymbol{W}_2} &= 2(U \pm c)\left(\frac{1}{\rho} \mp \frac{\gamma(\gamma-1)u}{2\rho c}\right) \\
\frac{\partial f_2^{\pm}}{\partial \boldsymbol{W}_3} &= 2(U \pm c)\left(\pm\frac{\gamma(\gamma-1)}{2\rho c}\right)
\end{aligned}
\tag{A.5}
$$

For $f_3^{\pm}$

$$
\begin{aligned}
\frac{\partial f_3^{\pm}}{\partial \boldsymbol{W}_1} &= \frac{u}{\gamma\rho} \pm \frac{\gamma(\gamma-1)(u^2 - E)}{\gamma\rho c} - \frac{u}{\rho} \\
\frac{\partial f_3^{\pm}}{\partial \boldsymbol{W}_2} &= -\frac{1}{\gamma\rho u} \mp \frac{\gamma(\gamma-1)u}{\gamma\rho c} + \frac{1}{\rho} \\
\frac{\partial f_3^{\pm}}{\partial \boldsymbol{W}_3} &= \pm\frac{\phi - 1}{\rho c}
\end{aligned}
\tag{A.6}
$$

For $f_{41}^{\pm}$

$$\begin{aligned}
\frac{\partial f_{41}^{\pm}}{\partial \boldsymbol{W}_1} &= \frac{1}{1+\gamma}\left(\pm\left\{\frac{\gamma(\gamma+1)(u^2-E)U}{\rho c} - \frac{2uc}{\rho}\right\} + \frac{2uU}{\rho}\right) \\
\frac{\partial f_{41}^{\pm}}{\partial \boldsymbol{W}_2} &= \frac{1}{1+\gamma}\left(\pm\left\{\frac{2c}{\rho} - \frac{\gamma(\gamma-1)uU}{\rho c}\right\} - 2\frac{U}{\rho}\right) \\
\frac{\partial f_{41}^{\pm}}{\partial \boldsymbol{W}_3} &= \pm\frac{\gamma(\gamma-1)U}{\rho c(1+\gamma)}
\end{aligned} \tag{A.7}$$

For f_{42}

$$\begin{aligned}
\frac{\partial f_{42}}{\partial \boldsymbol{W}_1} &= \frac{2\gamma(u^2-E)}{\rho(1+\gamma)} \\
\frac{\partial f_{42}}{\partial \boldsymbol{W}_2} &= -\frac{2\gamma u}{\rho(1+\gamma)} \\
\frac{\partial f_{42}}{\partial \boldsymbol{W}_3} &= \frac{2\gamma}{\rho(1+\gamma)}
\end{aligned} \tag{A.8}$$

For f_{43}

$$\begin{aligned}
\frac{\partial f_{43}}{\partial \boldsymbol{W}_1} &= -\frac{u^2}{\rho} \\
\frac{\partial f_{43}}{\partial \boldsymbol{W}_2} &= \frac{u}{\rho} \\
\frac{\partial f_{43}}{\partial \boldsymbol{W}_3} &= 0
\end{aligned} \tag{A.9}$$

And for $f_{44}^{\pm}$

$$\begin{aligned}
\frac{\partial f_{44}^{\pm}}{\partial \boldsymbol{W}_1} &= -\frac{w}{\gamma}\left(-\frac{u}{\rho} \mp \frac{\gamma(\gamma-1)(u^2-E)}{\rho c}\right) \\
\frac{\partial f_{44}^{\pm}}{\partial \boldsymbol{W}_2} &= -\frac{w}{\gamma}\left(\frac{1}{\rho} \pm \frac{\gamma(\gamma-1)u}{\rho c}\right) \\
\frac{\partial f_{44}^{\pm}}{\partial \boldsymbol{W}_3} &= -\frac{w}{\gamma}\left(\mp\frac{\gamma(\gamma-1)}{\rho c}\right)
\end{aligned} \tag{A.10}$$

Appendix B. Partial derivatives to the mesh velocity

The derivatives of the Van Leer fluxes to the mesh velocity w read

$$\begin{aligned}
\frac{\partial \Phi_1^{\pm}}{\partial w} &= f_1^{\pm}\frac{\partial f_2^{\pm}}{\partial w} \\
\frac{\partial \Phi_2^{\pm}}{\partial w} &= f_3^{\pm}\frac{\partial \Phi_1^{\pm}}{\partial w} + \Phi_1^{\pm}\frac{\partial f_3^{\pm}}{\partial w} \\
\frac{\partial \Phi_3^{\pm}}{\partial w} &= f_4^{\pm}\frac{\partial \Phi_1^{\pm}}{\partial w} + \Phi_1^{\pm}\frac{\partial f_4^{\pm}}{\partial w}
\end{aligned} \tag{B.1}$$

The functions f are defined in Eq. (A.2). The partial derivatives are for $f_2^{\pm}$

$$\frac{\partial f_2^{\pm}}{\partial w} = -2(U \pm c) \tag{B.2}$$

For $f_3^{\pm}$

$$\frac{\partial f_3^{\pm}}{\partial w} = \frac{1}{\gamma} \tag{B.3}$$

And for $f_4^{\pm}$

$$\frac{\partial f_4^{\pm}}{\partial w} = 2\frac{U \mp c}{1+\gamma} - \frac{U + w \mp 2c}{\gamma} \tag{B.4}$$

References

[1] O.O. Bendiksen, Fluid–structure coupling requirements for time accurate aeroelastic simulations, in: P.P. Freidmann and M.P. Païdoussis, eds., AD-Vol. 53-3, 4th Int. Symp. on Fluid–Structure Interaction, Aeroelasticity, Flow-Induced Vibrations and Noise, Dallas (1997).

[2] K.C. Park, C.A. Felippa and J.A. DeRuntz, Stabilisation of staggered solution procedures for fluid–structure interaction analysis, Comput. Methods Fluid–Structure Interaction Problems, AMD 26 (1977).

[3] B.B. Prananta, M.H.L. Hounjet and R.J. Zwaan, Thin layer Navier Stokes solver and its application for aeroelastic analysis of an airfoil in transonic flow, International Forum on Aeroelasticity and Structural Dynamics (Manchester, 1995).

[4] B.B. Prananta and M.H.L. Hounjet, Aeroelastic simulation with advanced CFD methods in 2D and 3D transonic flow, Proc. Unsteady Aerodynamics Conference Royal Aeronautical Society, London (1996).

[5] J. Mouro, Interactions fluide structure en frands déplacements, résolution numérique et application aux composants hydrauliques automobiles, Ph.D. Thesis, Ecole Polytechnique, France (1996).

[6] S. Piperno, Staggered time-integration methods for a one-dimensional Euler aeroelastic problem, Rapport de Recherche CERMICS 94-33 (1994).

[7] S. Piperno, Simulation numérique de phénomènes d'interaction fluide–structure, Ph.D. Thesis, Ecole Nationale Des Ponts et Chaussées, France (1995).

[8] F.J. Blom and P. Leyland, Analysis of fluid–structure interaction on moving airfoils by means of an improved ALE-method, AIAA Paper 97-1770 (1997).

[9] F.J. Blom and P. Leyland, Analysis of fluid–structure interaction by means of dynamic unstructured meshes, in: Païdoussis et al., eds., AD-Vol. 53-1, 4th Int. Symp. on Fluid–Structure Interaction, Aeroelasticity, Flow-Induced Vibrations and Noise, Dallas (1997) 3–10.

[10] S. Piperno, C. Farhat and B. Larrouturou, Partitioned procedures for the transient solution of coupled aeroelastic problems. part I: Model problem, theory and two-dimensional application, Comput. Methods Appl. Mech. Engrg. 124 (1995) 79–112.

[11] C. Farhat, N. Maman and M. Lesoinne, Mixed explicit/implicit time integration of coupled aeroelastic problems: three-field formulation, geometric conservation law and distributed solution, Center for Aerospace Structures 94-17, University of Colorado (1994).

[12] B.B. Prananta and M.H.L. Hounjet, Large time step aero-structural coupling procedures for aeroelastic simulation, Proc. 1997 International Forum on Aeroelasticity and Structural Dynamics, Vol. II, AIDAA, Rome (1997) 63–70.

[13] M.B. Giles, Stability and accuracy of numerical boundary conditions in aeroelastic analysis, Int. J. Numer. Methods Fluids 24 (1997) 739–757.

[14] M.B. Giles, Stability analysis of numerical interface conditions in fluid–structure thermal analysis, Int. J. Numer. Methods Fluids 25 (1997) 421–436.

[15] O.O. Bendiksen, A new approach to computational aeroelasticity, AIAA Paper 91-0939-CP (1991).

[16] L. He, Integration of 2-D fluid/structure coupled system for calculations of turbomachinery aerodynamic/aeroelastic instabilities, Int. Journal Comput. Fluid Dyn. 3 (1994) 217–231.

[17] J.J. Alonso and A. Jameson, Fully-implicit time-marching aeroelastic solutions, AIAA Paper 94-0056 (1994).

[18] R.B. Melville, S.A. Morton and D.P. Rizzetta, Implementation of a fully-implicit aeroelastic Navier–Stokes solver, AIAA Paper 97-2039 (1997).

[19] S.A. Morton, R.B. Melville and M.R. Visbal, Accuracy and coupling issues of aeroelastic Navier-Stokes solutions on deforming meshes, AIAA Paper 97-1085 (1997).

[20] C. Hirsch, Numerical Computation of Internal and External Flows, Vol. 2 (Wiley and Sons, 1990).

[21] C. Hirsch, Numerical Computation of Internal and External Flows, Vol. 1 (Wiley and Sons, 1988).

[22] J. Donea, S. Giuliani and J.P. Halleux, An arbitrary Lagrangian–Eulerian finite element method for transient dynamic fluid–structure interactions, Comput. Methods Appl. Mech. Engrg. 33 (1982) 689–723.

[23] J.T. Batina, Implicit flux-split Euler schemes for unsteady aerodynamic analysis involving unstructured dynamic meshes, AIAA J. 29(11) (1991) 1836–1843.

[24] K.J. Bathe and E.L. Wilson, Numerical Methods in Finite Element Analysis (Prentice-Hall, Englewood Cliffs, NJ, 1976).

[25] C. Farhat, High Performance Simulation of Coupled Nonlinear Transient Aeroelastic Problems (Cosmase Course, EPF-Lausanne, 1995).

[26] S. Piperno, Two-dimensional Euler aeroelastic simulations with interface matching relaxation, Proc. Second ECCOMAS Conference on Numer. Methods in Engineering (1996) 898-904.

[27] R.D. Rausch, J.T. Batina and H.T.Y. Yang, Euler flutter analysis of airfoils using unstructured dynamic meshes, AIAA Paper 89-1384-CP (1989).

[28] C. Farhat and T.Y. Lin, A structure attached corotational fluid grid for transient aeroelastic computations, AIAA J. 31(3) (1993) 597–599.

[29] F.F. Felker, A new method for transonic static aeroelasticity problems, AIAA Paper 92-2123-CP (1992).

[30] F.F. Felker, Direct solution of two-dimensional Navier-Stokes equations for static aeroelasticity problems, AIAA J. 31(1) (1993) 148–153.

[31] P.D. Thomas and C.K. Lombard, Geometric conservation law and its application to flow computations on moving grids, AIAA J. 17(10) (1979) 1030–1037.

[32] M. Lesoinne and C. Farhat, Geometric conservation laws for flow problems with moving boundaries and deformable meshes, and their impact on aeroelastic computations, Comput. Methods Appl. Mech. Engrg. 134 (1996) 71–90.

[33] B. Van Leer, Flux-vector splitting for the Euler equations, in: 8th International Conference on Numerical Methods in Fluid Dynamics (Springer-Verlag, 1982).